Supporting Information

Size and Rigidity of Cylindrical Polymer Brushes Dictate Long Circulating Properties *in vivo*

Markus Müllner,[†, #] *Sarah J. Dodds,*[†, #] *Tri-Hung Nguyen,*[+,#] *Danielle Senyschyn,*[+,#] *Christopher J. H. Porter,*[+,#] *Ben J. Boyd,*[+,#] *and Frank Caruso*[†,#,]*

[†]Department of Chemical and Biomolecular Engineering, The University of Melbourne, Parkville 3010, Australia; [+]Drug Delivery Disposition and Dynamics, Monash Institute of Pharmaceutical Sciences, Monash University, Parkville 3052, Australia; [#]ARC Centre of Excellence in Convergent Bio-Nano Science and Technology.

***Address correspondence to** fcaruso@unimelb.edu.au, ben.boyd@monash.edu.au, chris.porter@monash.edu.

S1. Synthetic procedure for the step-wise build-up of CPBs

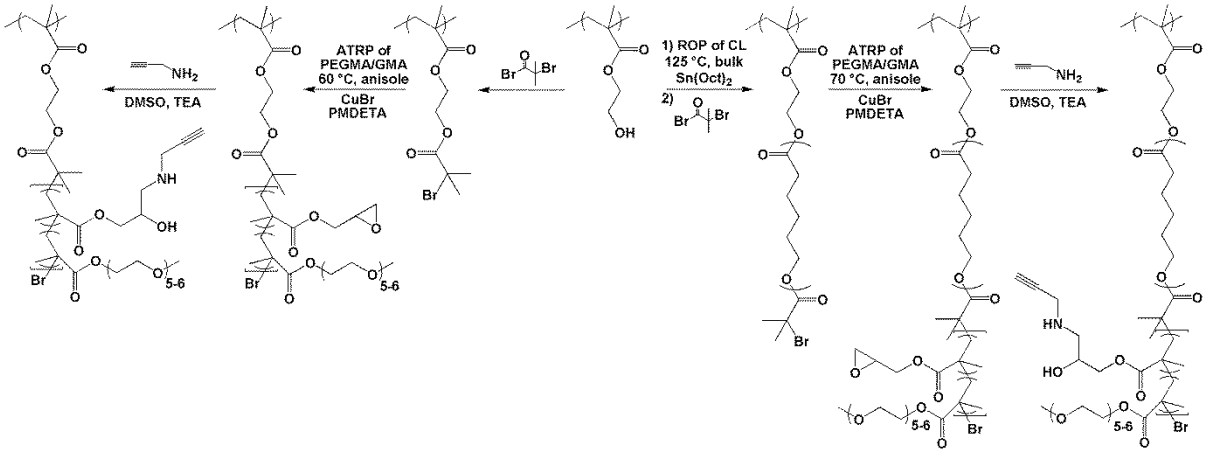

Figure S1. Step-wise build-up of clickable PEG-based CPBs.

S2. IR measurements

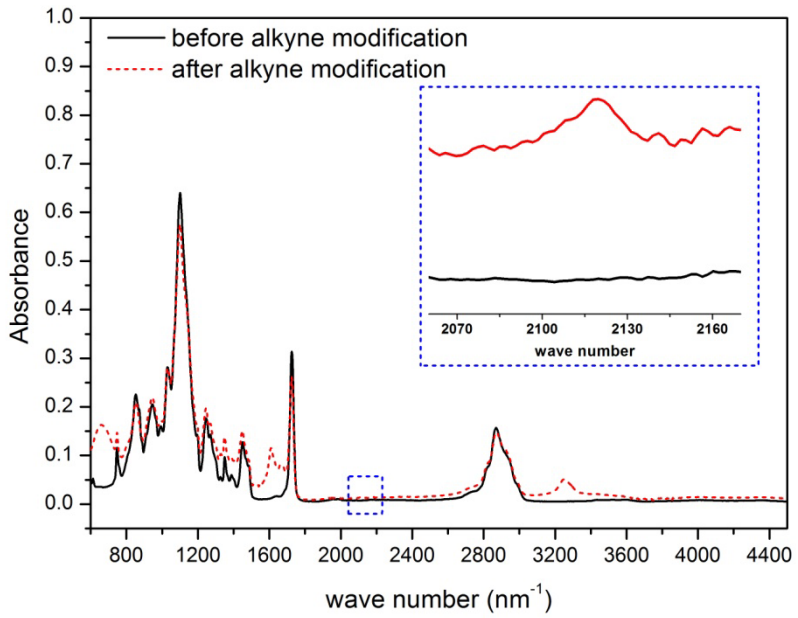

Figure S2. IR spectra of $[PEGMA_{140}\text{-}co\text{-}GMA_{21}]_{112}$ CPBs before (black solid line) and after (red dashed line) modification with propargylamine.

S3. Radiolabel attachment

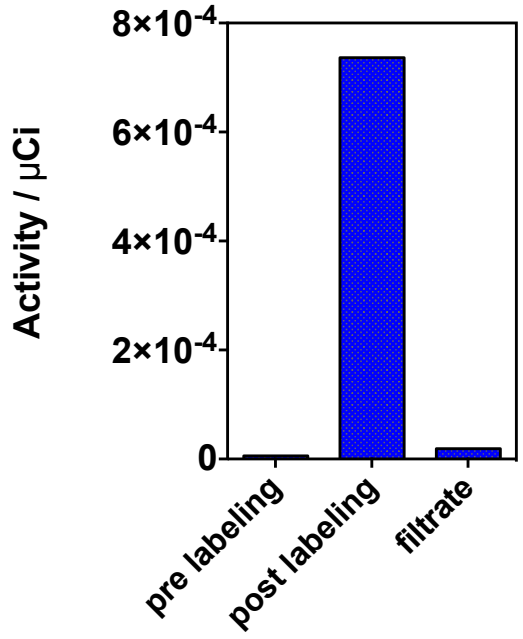

Figure S3. Activity of [PEGMA$_{140}$-*co*-GMA$_{21}$]$_{112}$ samples pre- and post-modification with radiolabel, as measured by liquid scintillation counting. Also shown is the activity of the filtrate after the labeled sample was passed through a 300 kDa MWCO centrifugal device.

S4. Dynamic Light Scattering (DLS) of [PEGMA$_{140}$-*co*-GMA$_{21}$]$_{112}$

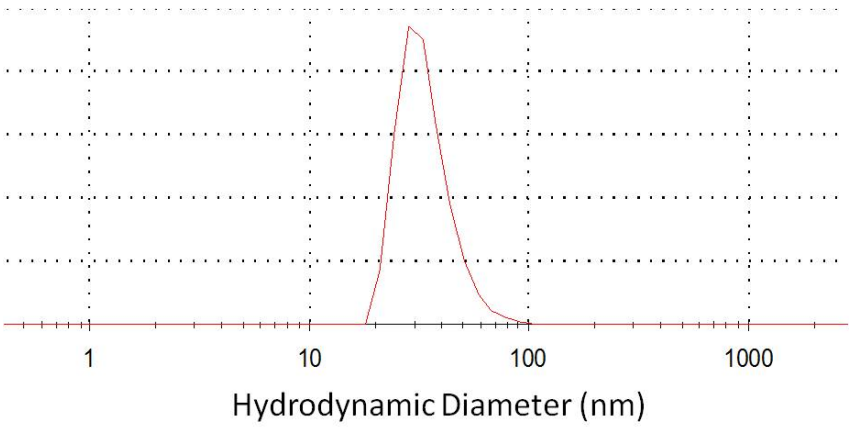

Figure S4. Number-weighted DLS of an aqueous suspension of [PEGMA$_{140}$-*co*-GMA$_{21}$]$_{112}$.

S5. AFM height and phase images of CPBs (including corresponding cross sections)

The cross sectional heights of the CPBs decrease for all samples due to flattening. Similarly, the phase images, typical for CPBs, underline the flattening of the brushes on mica. The appearance of flattened CPBs strongly depends on whether the CPB is fully amorphous or contains a PCL core. Taken this into account, the overall thicknesses of CPBs are indeed similar (taken into account the tip sample convolution phenomena).

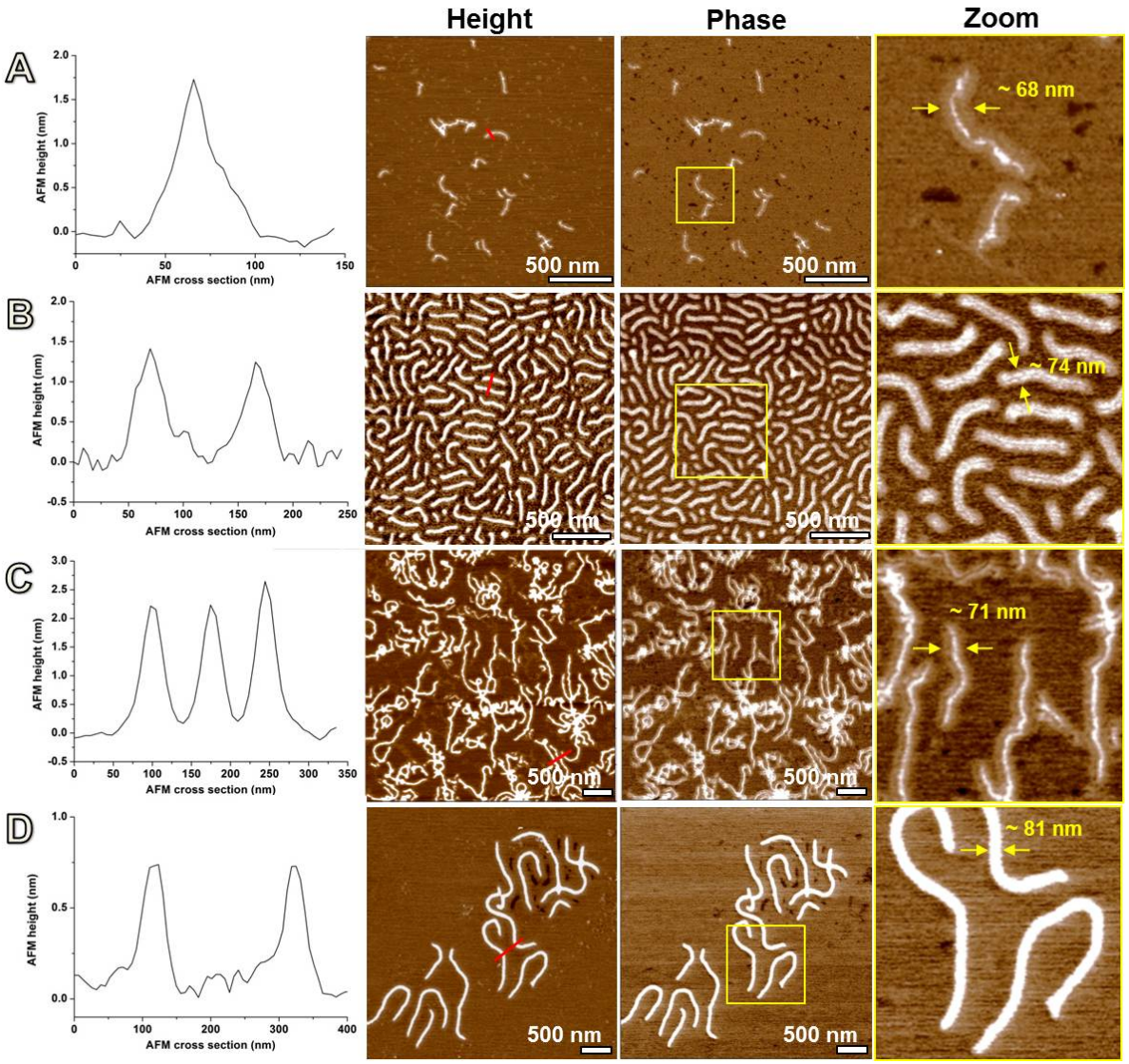

Figure S5. Cross sections (red line), including AFM height and phase images of air-dried CPBs deposited from acetone on mica: (A) $[PEGMA_{188}\text{-}co\text{-}GMA_{32}]_{2700}$, (B) $[PCL_{25}\text{-}b\text{-}(PEGMA_{98}\text{-}co\text{-}GMA_{16})]_{2700}$, (C) $[PEGMA_{170}\text{-}co\text{-}GMA_{28}]_{7500}$, and (D) $[PCL_{14}\text{-}b\text{-}(PEGMA_{94}\text{-}co\text{-}GMA_{16})]_{7500}$, respectively.

S6. DSC measurements of PCL brushes

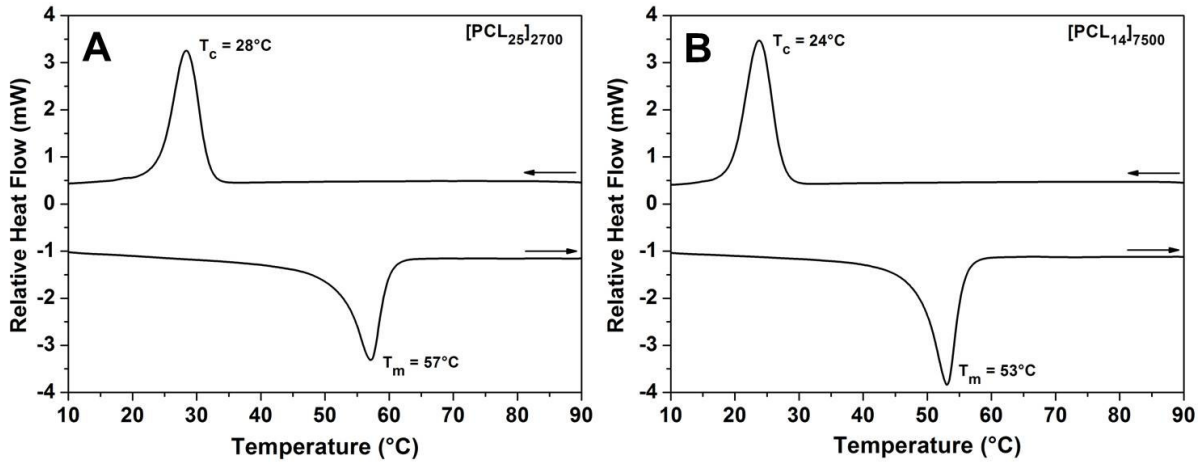

Figure S6. DSC measurements of (A) $[PCL_{25}]_{2700}$ and (B) $[PCL_{14}]_{7500}$.

S7. AFM height images of CPBs (deposited from water)

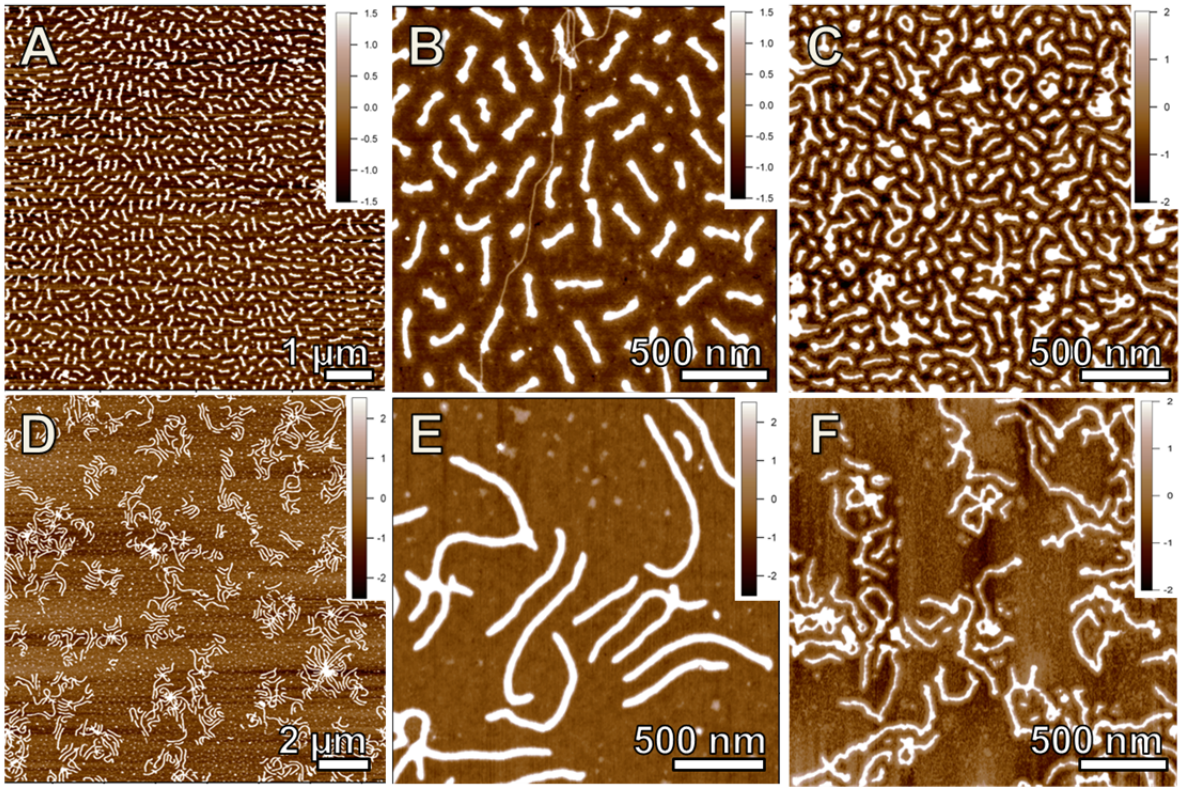

Figure S7. AFM height images of air-dried CPBs deposited from water on mica: (A,B) $[PCL_{25}$-*b*-$(PEGMA_{98}$-*co*-$GMA_{16})]_{2700}$, (C) $[PEGMA_{188}$-*co*-$GMA_{32}]_{2700}$, (D,E) $[PCL_{14}$-*b*-$(PEGMA_{94}$-*co*-$GMA_{16})]_{7500}$, and (F) $[PEGMA_{170}$-*co*-$GMA_{28}]_{7500}$, respectively.

S8. *In vitro* cell association of CPBs (0.05g·L^{-1})

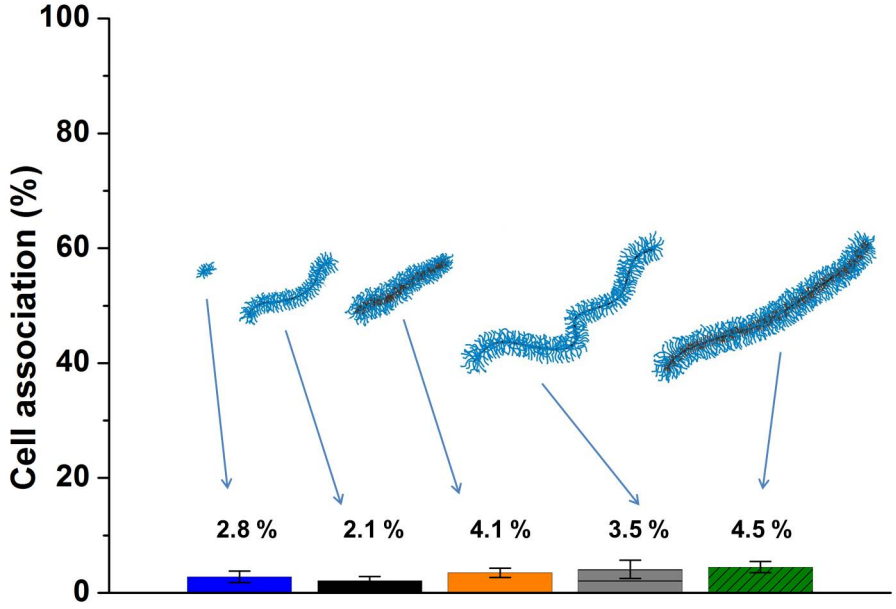

Figure S8. Cell association of AF647-labeled CPBs after 24 h incubation (conc. = 0.05 g·L^{-1}) with RAW 264.7 cells (quantified by flow cytometry).

S9 Additional deconvolution microscopy

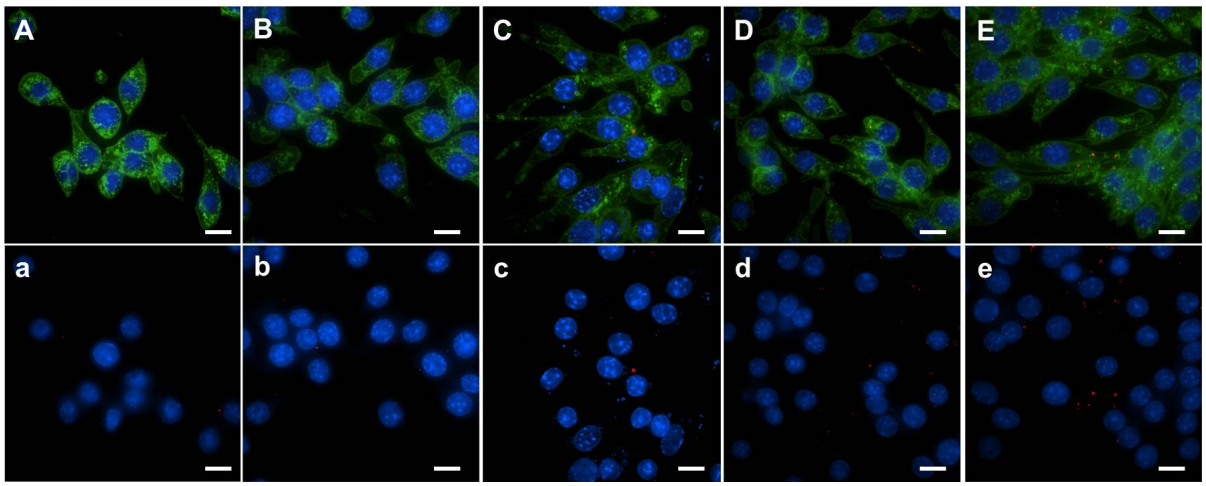

Figure S9. Deconvolution images of RAW cells (with **(A-E)** and without **(a-e)** membrane stain) incubated with AF647-labeled CPBs (conc. = 0.2 g·L^{-1}, 24 h). **(A,a)** [PEGMA$_{140}$-*co*-GMA$_{21}$]$_{112}$, **(B,b)** [PEGMA$_{188}$-*co*-GMA$_{32}$]$_{2700}$, **(C,c)** [PCL$_{25}$-*b*-(PEGMA$_{98}$-*co*-GMA$_{16}$)]$_{2700}$, **(D,d)** [PEGMA$_{170}$-*co*-GMA$_{28}$]$_{7500}$, and **(E,e)** [PCL$_{14}$-*b*-(PEGMA$_{94}$-*co*-GMA$_{16}$)]$_{7500}$, respectively. The scale bars represent 10 µm.

S10. Overview of various CPBs used for *in vivo* studies

Table S1. Overview of various CPBs used for *in vivo* studies.

	Composition[1]	**Backbone**	**1.Block**	**2.Block**	**MW**[4] ($t \cdot mol^{-1}$)
A	$[PEGMA_{140}\text{-}co\text{-}GMA_{21}]_{112}$	[2]$PBIEM_{112}$	ATRP	-	5
B	$[PEGMA_{188}\text{-}co\text{-}GMA_{32}]_{2700}$	[3]$PBIEM_{2700}$	ATRP	-	164
C	$[PEGMA_{170}\text{-}co\text{-}GMA_{28}]_{7500}$	[3]$PBIEM_{7500}$	ATRP	-	412
D	$[PCL_{25}\text{-}b\text{-}(PEGMA_{98}\text{-}co\text{-}GMA_{16})]_{2700}$	[3]$PHEMA_{2700}$	ROP	ATRP	93
E	$[PCL_{14}\text{-}b\text{-}(PEGMA_{94}\text{-}co\text{-}GMA_{16})]_{7500}$	[3]$PHEMA_{7500}$	ROP	ATRP	240

[1] Determined by ^{1}H NMR as detailed in the Experimental Section. [2] Synthesized using ATRP. [3] Synthesized using anionic polymerization. [4] Molecular weight (MW) determined by ^{1}H NMR.